

Macrocyclic Ligands

Calix[4]pyrrolato Aluminates: The Effect of Ligand Modification on the Reactivity of Square-Planar Aluminum Anions

Fabian Ebner, Philipp Mainik, and Lutz Greb*^[a]

Abstract: Structural constraint represents an attractive tool to modify *p*-block element properties without the need for unusual oxidation or valence states. The recently reported methyl-calix[4]pyrrolato aluminate established the effect of forcing a tetrahedral aluminum anion into a square-planar coordination mode. However, the generality of this structural motif and any consequence of ligand modification remained open. Herein, a systematic ligand screening was launched, and the class of square-planar aluminum anions was extended by two derivatives that differ in the *meso*-substitution at the calix[4]pyrrolato ligand. Strikingly, this modification provoked opposing trends in the preference for a Lewis acidic binding mode with σ -donors versus the aluminum-ligand cooperative binding mode with carbonyls. Insights into the origin of these counterintuitive experimental observations were provided by computation and bond analysis. Importantly, this rationale might allow to exploit mode-selective binding for catalytic rate control.

During recent years, structurally constrained *p*-block element compounds evolved from non-VSEPR (valence shell electron pair repulsion) curiosities to conceptual drivers for bond activation and catalysis.^[1] Besides the more established trigonal group 15,^[2] or pyramidalized group 13 species,^[1f,3] the field of the planarization of tetrahedrons developed only recently. Challenged by the substantially preferred tetrahedral van't Hoff-Le Bel configuration of 8-valence electron species, planarized anti-van't Hoff-Le Bel main group elements were pursued for a long time.^[4] Although the successful isolation of some derivatives satisfied structural interests, the consequences of planarization on the properties of these compounds, and potential applications, remained largely unexplored.^[5] Early theoretic

studies disclosed an energetic lowering of the lowest unoccupied molecular orbital (LUMO) and its p_z -type character at the central, planar element upon planarization.^[6] Indeed, the hereby induced increase of Lewis acidity was confirmed experimentally for silicon and the isoelectronic aluminate using the *meso*-octamethyl-calix[4]pyrrolato ligand ("methyl-calix[4]pyrrolato", Figure 1 A).^[7] The square-planar aluminate [1][−] represents a rare anionic Lewis acid with untapped potential in charge-discriminating bond activation.^[8] In addition to mere planarization, the ligand enabled highly reversible element-ligand cooperative (ELC) reactivity with carbonyls.^[9] Beyond elucidation of mechanistic details and applications in hydroboration catalysis, the system was extended towards alcohols, disclosing a generality of ELC by O–H-bond activation.^[10]

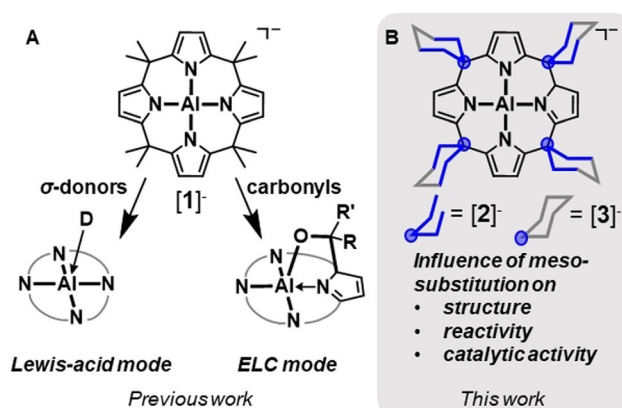


Figure 1. (A) The recently introduced *meso*-octamethylcalix[4]pyrrolato aluminate [1][−] and its interaction with substrates. (B) The herein studied ligand modification at the *meso*-position, which modulates the binding tendency of σ -donors and carbonyls.

Overall, ELC gains momentum in bond activation with earth-abundant main group elements as an alternative for transition metals.^[11] Controlling both aspects, planarization induced reactivity and ELC, by defined and well understood changes is vital for further developing these promising fields. Herein, we provide the synthesis of two new planar aluminates and a comparison of structure and reactivity with the methyl-calix[4]pyrrolato aluminate, [PPh₄][1]. It allows concluding how ligand modification steers the preferred form of substrate binding and offers a handle for substrate activation in catalytic transformations.

The syntheses of the two new aluminates, ethyl-substituted [PPh₄][2] and cyclohexyl-substituted [PPh₄][3] were performed

[a] F. Ebner, P. Mainik, Dr. L. Greb
Anorganisch-Chemisches Institut
Ruprecht-Karls-Universität Heidelberg
Im Neuenheimer Feld 270, 69120 Heidelberg (Germany)
E-mail: greb@uni-heidelberg.de

Supporting Information and the ORCID identification number(s) for the author(s) of this article can be found under:
<https://doi.org/10.1002/chem.202005493>.

© 2021 The Authors. Published by Wiley-VCH GmbH. This is an open access article under the terms of the Creative Commons Attribution Non-Commercial License, which permits use, distribution and reproduction in any medium, provided the original work is properly cited and is not used for commercial purposes.

in dimethoxyethane (DME) by stirring the ethyl-calix[4]pyrrole/cyclohexyl-calix[4]pyrrole with 2 equiv. of LiAlH_4 for 24 h at 90°C , obtaining the corresponding dianionic hydrido aluminates (see the Supporting Information). Salt metathesis with PPh_4Cl in CH_2Cl_2 induced the precipitation of LiH and allowed the isolation of the donor-free aluminates after purification in 96% yield for $[\text{PPh}_4][\mathbf{2}]$ and 33% for $[\text{PPh}_4][\mathbf{3}]$. On the NMR-time scale, both aluminates possess peak patterns that agree with an averaged D_{2d} symmetry. Suitable crystals for single-crystal X-ray diffraction (SCXRD) were obtained from a saturated CH_2Cl_2 solution at -40°C for $[\text{PPh}_4][\mathbf{2}]$ and a diethyl ether solution for $[\text{PPh}_4][\mathbf{3}]$ under the same conditions (Figure 2).

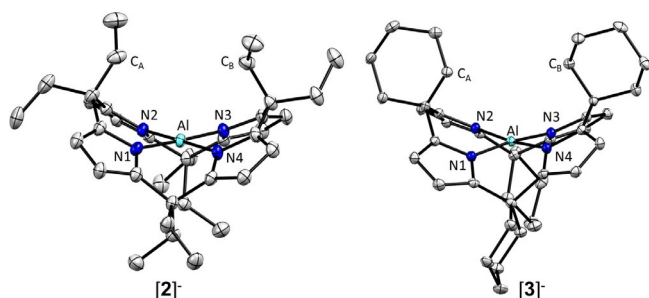


Figure 2. Molecular structure of the aluminates **2** and **3**. Hydrogen atoms and cations are omitted for clarity. Displacement ellipsoids are drawn with a probability of 50%. Selected bond lengths [pm] and bond angles [$^\circ$]: **2**: Al–N(1) 188.3(2), Al–N(2) 188.5(2), Al–N(3) 187.9(2), Al–N(4) 188.6(2), N(1)–Al–N(3) 179.04(10), N(2)–Al–N(4) 178.05(10). **3**: Al–N(1/2/3/4) 187.8(15), N(1)–Al–N(3)/N(2)–Al–N(4) 172.69(11).

Whereas the aluminate $[\mathbf{2}]^-$ manifested planarity with a $179.04(10)^\circ$ N(1)–Al–N(3) $178.05(10)^\circ$ N(2)–Al–N(4) angle lying in the same region as the methyl derivative $[\mathbf{1}]^-$, the aluminate $[\mathbf{3}]^-$ exhibited a $172.69(11)^\circ$ N(1)–Al–N(3) and $178.05(10)^\circ$ N(2)–Al–N(4) angle. Parametrization of the planarity by the τ_4 value^[12] showed just a slight increase from ideal $\tau=0$ (D_{4h}) to 0.02 for $[\mathbf{2}]^-$, but of 0.10 for $[\mathbf{3}]^-$ (compared to 0.01 for $[\mathbf{1}]^-$). The slight distortion of $[\mathbf{3}]^-$ by about 7° from ideal square-planarity indicates a generally shallow potential energy surface for the planarization coordinate. The Al–N average bond lengths of $[\mathbf{2}]^-$ and $[\mathbf{3}]^-$ are similar {Al– N_{avg} $[\mathbf{2}]^-$: 188.3(2) pm; $[\mathbf{3}]^-$: 187.8(15) pm} and in good agreement with $[\mathbf{1}]^-$ [189.2(2) pm]. A further structural parameter, indicating the accessibility of the Al-central atom, is obtained by the distance of the inward orientated carbon atoms of the *meso*-alkyl substituents (see C_A – C_B in Figure 2). $[\mathbf{1}]^-$: 457.9 pm, $[\mathbf{2}]^-$: 420.0 pm, $[\mathbf{3}]^-$: 430.3 pm). Only considering this parameter, the methyl-substituted derivative $[\mathbf{1}]^-$ seems to be the most easily accessible.

To answer the question whether the differences in the structures of $[\mathbf{1}]^-$, $[\mathbf{2}]^-$, and $[\mathbf{3}]^-$ are influencing their reactivity, both new aluminates were subjected to a σ -donor (THF) and the results compared with that for the methyl derivative $[\text{PPh}_4][\mathbf{1}]$.^[7a] Thus, both ($[\text{PPh}_4][\mathbf{2}]$ or $[\text{PPh}_4][\mathbf{3}]$) were stirred in THF, precipitated with *n*-hexane, and dried under reduced pressure. In comparison to $[\text{PPh}_4][\mathbf{1}]$, which forms the mono-THF-adduct under the same conditions, $[\mathbf{2}]^-$ led to a bis-THF-adduct,

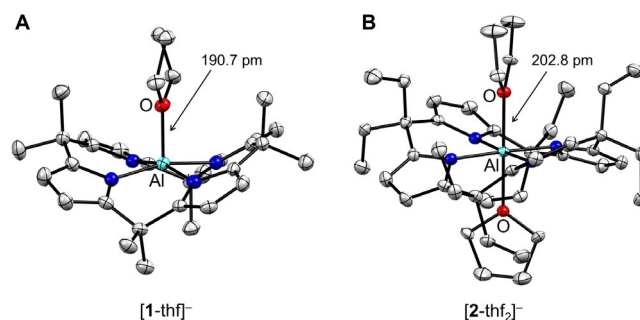


Figure 3. Molecular structure of the (A) mono-thf-adduct of $[\mathbf{1}]^-$ and (B) the bis-THF-adduct of $[\mathbf{2}]^-$. Hydrogen atoms and cations are omitted for clarity. Displacement ellipsoids are drawn with a probability of 50%. Selected bond lengths [pm] and bond angles [$^\circ$]: $[\text{Li}(\text{thf})_4][\mathbf{1}\text{-thf}]^-$: Al– N_{avg} 195.8(2), Al–O 191.5(2), N1–Al–N3 165.7(1), N2–Al–N4 164.6(1). $[\text{Li}(\text{thf})_4][\mathbf{2}\text{-(thf)}_2]^-$: Al– N_{avg} 199.3(2), Al–O 202.8(2), N(4)–Al(1)–N(2) 177.75(11), N(3)–Al(1)–N(1) 177.07(11).

whereas $[\mathbf{3}]^-$ revealed no THF-adduct formation. The solid-state structure of the bis-THF-adduct of $[\mathbf{2}]^-$ was compared with the mono-THF-adduct of $[\mathbf{1}]^-$ (Figure 3).

The Al– N_{avg} bond length in $[\mathbf{2}\text{-(thf)}_2]^-$ is elongated by 11 pm compared to free aluminate $[\mathbf{2}]^-$, significantly more than the bond length increase (7 pm) upon mono-THF coordination to $[\mathbf{1}]^-$. Accordingly, the Al–O-bond lengths in $[\mathbf{2}\text{-(thf)}_2]^-$ are 12 pm longer than in the mono-THF-adduct $[\mathbf{1}\text{-thf}]^-$.

To investigate the aluminum-ligand cooperative binding of C=O containing substrates (“ELC-mode, Figure 1”), CO_2 and *para*-methylbenzaldehyde (*p*MBA) were subjected to $[\text{PPh}_4][\mathbf{2}]$ and $[\text{PPh}_4][\mathbf{3}]$. In all four cases, the expected ELC-mode was identified by a characteristic color change of the reaction mixture, dearomatized pyrrole rings in the ^1H NMR spectra, and SCXRD diffraction analysis (Figure 4 and Supporting Information). Comparison of the structural parameters of $[\text{PPh}_4][\mathbf{1}^*\text{-pMBA}]$ with $[\text{PPh}_4][\mathbf{2}^*\text{-pMBA}]$ showed no significant differences in bond length or bond angles [e.g., Al1–O1: 179.0 for $[\mathbf{1}^*]^-$; 179.6 for $[\mathbf{2}^*]^-$; C1–C29 ($[\mathbf{1}^*]^-$): 159.6; C1–C37 $[\mathbf{2}^*]^-$: 159.6, * indicates a species with dearomatized ligand]. Hence, from the structural perspective no clear-cut indications for a distinct reactivity of $[\mathbf{1}]^-$ and $[\mathbf{2}]^-$ against carbonyls were extractable. Therefore, a competitive experiment between $[\mathbf{1}]^-$ and $[\mathbf{2}]^-$ with *p*MBA was carried out in CD_2Cl_2 . To a 1:1 mixture of $[\text{PPh}_4][\mathbf{1}]$ and $[\text{PPh}_4][\mathbf{2}]$, 1 equiv. of *p*MBA (relative to $[\text{PPh}_4][\mathbf{1}]$) was added, and quantitative conversion to $[\text{PPh}_4][\mathbf{1}^*\text{-pMBA}]$ was observed, indicating $[\mathbf{1}]^-$ as the stronger ELC-agent for this type of aldehyde. Indeed, a quantitative transfer of *p*MBA was also observed upon adding 1 equiv. of $[\text{PPh}_4][\mathbf{1}]$ to $[\text{PPh}_4][\mathbf{2}^*\text{-pMBA}]$. Mixing $[\text{PPh}_4][\mathbf{3}^*\text{-pMBA}]$ with $[\text{PPh}_4][\mathbf{2}]$ yielded an equilibrium of both * -adducts, with an equilibrium constant of $K=0.12$ in favor of $[\text{PPh}_4][\mathbf{3}^*\text{-pMBA}]$. These experimental observations certainly raised some more questions as the affinity of the planar aluminates against THF (a σ -donor) appeared to be in the order $[\mathbf{3}]^- < [\mathbf{1}]^- < [\mathbf{2}]^-$. This trend might be explained by aluminum planarization and the hereby lowered LUMO energy, which diminishes from $[\mathbf{3}]^- > [\mathbf{1}]^- > [\mathbf{2}]^-$ (Table S4). However, against *p*MBA (an ELC-binder), the order $[\mathbf{2}]^- < [\mathbf{3}]^- < [\mathbf{1}]^-$ occurred, indicating other factors governing the trend.

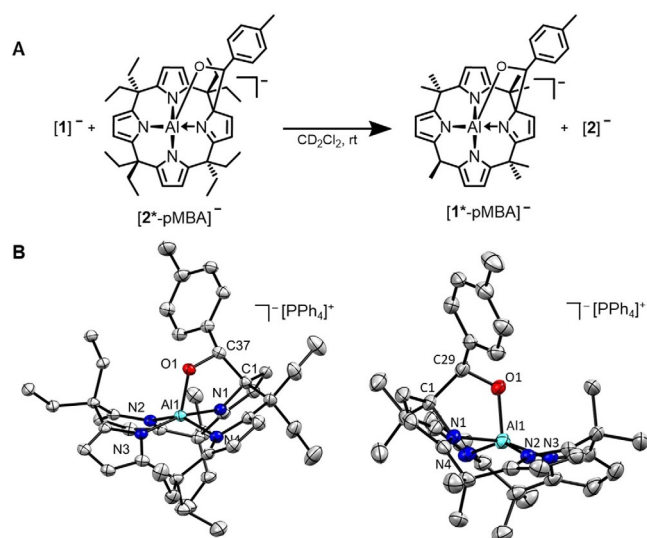


Figure 4. (A) Quantitative substrate transfer (*pMBA*) from $[2^*-pMBA]^-$ to $[1]^-$. (B) Molecular structures of the *pMBA*-adducts of $[2]^-$ and $[1]^-$. Hydrogen atoms are omitted for clarity. Displacement ellipsoids are drawn with a probability of 50%. Selected bond lengths [pm]: $[PPh_4][2^*-pMBA]$: Al(1)–N(1) 197.90(17), Al(1)–N(2) 195.37(17), Al(1)–N(3) 192.46(17), Al(1)–N(4) 194.98(17), Al(1)–O(1) 179.63(15), O(1)–C(37) 142.7(3), C(1)–C(37) 159.6(3). $[PPh_4][1^*-pMBA]$: Al(1)–N(1) 197.2(3), Al(1)–N(2) 196.1(2), Al(1)–N(3) 191.5(3), Al(1)–N(4) 195.5(2), Al(1)–O(1) 179.0(2), O(1)–C(29) 141.0(3), C(1)–C(29) 159.6(4).

To rationalize these observations, computational methods were applied. First, the thermodynamics of THF and *pMBA* binding were computed at the reliable PW6B95-D3(BJ)/def2-QZVPP//PBEh-3c level of theory (Table 1, Col1).^[13] Indeed, negative Gibbs free formation energies were obtained for all adducts that were observed experimentally. Accordingly, positive energies were computed for the bis-THF adduct formation of $[1]^-$ and both THF bindings with $[3]^-$. Moreover, the addition of *pMBA* to $[1]^-$ is more favorable by 10 kJ mol⁻¹ than for $[2]^-$, well in line with the experimentally observed transfer reaction (Figure 4A). To identify the relevant contributions for adduct formation, the energies were considered without solvation and dispersion correction (Table 1, Cols2A/2B and Cols3A/3B), and the bonding between the fragments was studied by the energy decomposition analysis scheme (EDA).^[14] The THF binding will be discussed first. The empty *p*_z-type orbital located at the square-planar aluminum serves as acceptor for dative bonding in all cases.^[7b] As can be seen from the differences in binding free energies with and without solvation correction ($\Delta\Delta G_1 = \Delta G_{\text{solv},D3} - \Delta G_{\text{gas},D3}$, Table 1), solvation disfavors THF adduct formation with $[2]^-$ and $[3]^-$ by roughly 10 kJ mol⁻¹ more as it disfavors adduct formation with $[1]^-$. However, this is more than outweighed by the pronounced attractive dispersion interaction between $[2]^-$ and the THF units, as revealed by discarding dispersion correction ($\Delta\Delta G_2 = \Delta G_{\text{Gas},D3} - \Delta G_{\text{Gas}}$,

Table 1. Overview of quantum chemical data obtained from the calculation of the thermodynamics with various parameters (PW6B95-D3(BJ)/def2-QZVPP//PBEh-3c + COSMO-RS (CH₂Cl₂), PW6B95-D3(BJ)/def2-QZVPP//PBEh-3c, PW6B95/def2-QZVPP//PBEh-3c, and the differences that occur by omitting solvation and dispersion correction) and the energy decomposition analysis, EDA (BP86-D3(BJ)/TZ2P//PBEh-3c).

	ΔG [kJ mol ⁻¹]					EDA [kJ mol ⁻¹]		[%]		
	1) PW6B95-D3(BJ)/QZVPP + COSMO-RS	2A) PW6B95-D3(BJ)/QZVPP	2B) $\Delta\Delta G_1$ ($\Delta G_{\text{solv},D3} - \Delta G_{\text{gas},D3}$)	3A) PW6B95/QZVPP	3B) $\Delta\Delta G_2$ ($\Delta G_{\text{gas},D3} - \Delta G_{\text{gas}}$)	Dispersion energy	Deformation energy	Orbital	Electrostatic	Dispersion
$[1]^- + \text{THF} \rightarrow [1\text{-thf}]^-$	-12	-22	-10	10	32	-86	73	30	54	16
$[1]^- + 2\text{THF} \rightarrow [1\text{-thf}_2]^-$	-1	-36	-35	30	66	-	-	-	-	-
$[1\text{-thf}]^- + \text{THF} \rightarrow [1\text{-thf}_2]^-$	11	-13	-24	20	33	-87	53	29	52	19
$[1]^- + pMBA \rightarrow [1\text{-}pMBA]^-$	-11	-17	-6	20	37	-89	347	54	42	4
$[2]^- + \text{THF} \rightarrow [2\text{-thf}]^-$	-14	-33	-19	2	35	-91	62	30	53	17
$[2]^- + 2\text{THF} \rightarrow [2\text{-thf}_2]^-$	-33	-79	-46	-1	78	-	-	-	-	-
$[2\text{-thf}]^- + \text{THF} \rightarrow [2\text{-thf}_2]^-$	-18	-46	-28	-3	43	-98	33	28	51	21
$[2]^- + pMBA \rightarrow [2\text{-}pMBA]^-$	-1	-6	-5	39	45	-100	371	54	42	4
$[3]^- + \text{THF} \rightarrow [3\text{-thf}]^-$	9	-8	-17	25	33	-93	93	30	53	17
$[3]^- + 2\text{THF} \rightarrow [3\text{-thf}_2]^-$	43	-3	-46	67	70	-	-	-	-	-
$[3\text{-thf}]^- + \text{THF} \rightarrow [3\text{-thf}_2]^-$	35	6	-29	42	37	-95	66	29	51	20

Table 1), but less so for $[3]^-$. The dispersion majorly affects the binding of the second THF $\{[2-(\text{thf})]^- [2-(\text{thf})_2]^- \}$. Remarkably, in the percentual contributions on the binding energies revealed by EDA, dispersion makes up a significant proportion of up to 21 % of the overall interaction energy with THF. Non-covalent interaction (NCI) plot analysis illustrated the crucial attractive interactions with the THF unit between the outward-oriented ethyl groups in $[2-(\text{thf})_2]^-$. This interaction is absent in $[1-(\text{thf})_2]^-$ due to the shorter Me groups and in $[3]^-$ due to “tied-back” alkyl groups in the six-membered ring (see Figure S34). Still, the more attractive dispersion does not exhaustively explain the preference for bis-THF adduct with $[2]^-$. A closer look at the energy decomposition analysis (Table 1) disclosed smaller deformation energy for binding the second THF unit to $[2]$, ultimately causing the energetic difference. The origins of the deformation energy differences are difficult to pin down, but the critical point to keep in mind is: σ -adduct formation is favored for $[2]^-$ by less deformation energy and larger dispersion stabilization.

Next, the binding of *p*MBA was inspected for $[1]^-$ and $[2]^-$. In contrast to THF, solvation is not differentiating $[1]^-$ vs. $[2]^-$, but dispersion causes a preference of *p*MBA-binding for the ethyl derivative $[2]^-$. However, with a contribution of only 4 % (EDA), dispersion could not be accounted for as the decisive factor, but other factors were thought to be responsible. As a measure of the donor ability of the α -position in the ligand, the gas-phase proton affinity was computed (see Table S2), rendering $[2]^-$ as a stronger donor than $[1]^-$. Hence, both factors, dispersive attraction, and ligand donor ability are more favorable for $[2]^-$, but still, the global computed energies and the experimental observations render $[1]^-$ as the better ELC-agent. Again, it is the deformation energy that determines the outcome (Table 1, EDA), but this time, in the inverted order as for σ -adduct formation. For the ethyl derivative $[2]^-$, a deformation energy larger by 25 kJ mol^{-1} as for $[1]^-$ derogates the ELC-binding. Comparing the molecular structures of $[2^*-p\text{MBA}]^-$ with $[1^*-p\text{MBA}]^-$ illustrates allylic strain between the ethyl group and the β -pyrrole position as the most likely cause.^[15] The ELC-binding of the aldehyde forces the neighboring ethyl group in an unfavorable position—a situation that does not happen in the adduct $[1^*-p\text{MBA}]^-$.

Comparing the differences of σ -adduct formation and ELC-binding for $[1]^-$ and $[2]^-$, although seemingly subtle, offers an interesting consequence. Larger groups introduced in the *meso*-positions act dually: dispersion donors that favor the formation of σ -adducts but hinder the formation of the ELC-binding products by steric effects. This spatial control allows engineering the potential energy surface towards either one over the other binding mode. However, the question on the usefulness of this arises. In our recent study on the catalytic hydroboration of aldehydes with $[1]^-$, we realized that the ELC-binding mode acts as a type of decelerator or a temporal protecting group, whereas the reactive species for hydroboration seems to be the σ -adduct form.^[9] Hence, this allows for the assumption that $[2]^-$ (a preferential σ -binder) should be catalytically more active than $[1]^-$ (a preferential ELC-binder). Although a solid mechanistic elucidation is pending, this adds an

exciting perspective for catalyst rate control and regioselectivity in more complex substrates by the ligand periphery's steric profile.

The synthesis and isolation of two new aluminates derived from the calix[4]pyrrolato ligand allow to broaden and to rationalize the concept of element planarization and element-ligand cooperative effects. 1) The square planar coordination environment and the hereby induced anionic Lewis acidity, as well as the ability for element-ligand cooperative reactivities, is a general property of this substance class. 2) A fitting correlation between planarization, LUMO energy and THF-affinity indicates that structural constraint is a crucial factor that determines the reactivity. 3) Different substituents in the *meso*-position enable a subtle control of substrate binding modes. Dispersive interactions and lower deformation energies favor adduct formation with σ -donors for the ethyl-derivative $[2]^-$, whereas the steric demand in the periphery disfavors the ELC-binding mode at the same time. Overall, these studies pave the way for a better understanding of the electronic and steric features of the class of *p*-block calix[4]pyrrolato complexes and opens multiple ways to control their properties for further applications.

Experimental Section

Crystallographic data: Deposition numbers 2052818, 2052819, 2052820, and 2052821 contain the supplementary crystallographic data for this paper. These data are provided free of charge by the joint Cambridge Crystallographic Data Centre and Fachinformationszentrum Karlsruhe Access Structures service.

Acknowledgements

We thank Prof. H.-J. Himmel for his steady support. Financial support was provided by the DFG (Emmy-Noether program, GR 5007/2-1, L.G.) and the Foundation of German Business (sdw, F.E.). The BWFor/BWUniCluster are acknowledged for computational resources, funded by the DFG. Open access funding enabled and organized by Projekt DEAL.

Conflict of interest

The authors declare no conflict of interest.

Keywords: aluminum · anti-van't Hoff–Le Bel · calix[4]pyrrole · Lewis acid · planar aluminate

- [1] a) S. A. Culley, A. J. Arduengo, *J. Am. Chem. Soc.* **1984**, *106*, 1164–1165; b) N. L. Dunn, M. Ha, A. T. Radosevich, *J. Am. Chem. Soc.* **2012**, *134*, 11330–11333; c) T. P. Robinson, D. M. De Rosa, S. Aldridge, J. M. Goicoechea, *Angew. Chem. Int. Ed.* **2015**, *54*, 13758–13763; *Angew. Chem.* **2015**, *127*, 13962–13967; d) A. Hentschel, A. Brand, P. Wegener, W. Uhl, *Angew. Chem. Int. Ed.* **2018**, *57*, 832–835; *Angew. Chem.* **2018**, *130*, 840–843; e) M. B. Kindervater, K. M. Marczenko, U. Werner-Zwanziger, S. S. Chitnis, *Angew. Chem. Int. Ed.* **2019**, *58*, 7850–7855; *Angew. Chem.* **2019**, *131*, 7932–7937; f) A. Ben Saida, A. Chardon, A. Osi, N. Tumanov, J. Wouters, A. I. Adjieufack, B. Champagne, G. Berionni, *Angew. Chem. Int. Ed.* **2019**, *58*, 16889–16893; *Angew. Chem.* **2019**, *131*, 17045–

- 17049; g) J. Cui, Y. Li, R. Ganguly, A. Inthirarajah, H. Hirao, R. Kinjo, *J. Am. Chem. Soc.* **2014**, *136*, 16764–16767; h) S. Volodarsky, R. Dobrovetsky, *Chem. Commun.* **2018**, *54*, 6931–6934; i) F. Wang, O. Planas, J. Cornella, *J. Am. Chem. Soc.* **2019**, *141*, 4235–4240.
- [2] a) W. Zhao, S. M. McCarthy, T. Y. Lai, H. P. Yennawar, A. T. Radosevich, *J. Am. Chem. Soc.* **2014**, *136*, 17634–17644; b) T. P. Robinson, S.-K. Lo, D. De Rosa, S. Aldridge, J. M. Goicoechea, *Chem. Eur. J.* **2016**, *22*, 15712–15724; c) A. Brand, W. Uhl, *Chem. Eur. J.* **2019**, *25*, 1391–1404; d) M. Hirai, N. Tanaka, M. Sakai, S. Yamaguchi, *Chem. Rev.* **2019**, *119*, 8291–8331; e) K. Lee, A. V. Blake, A. Tanushi, S. M. McCarthy, D. Kim, S. M. Loria, C. M. Donahue, K. D. Spielvogel, J. M. Keith, S. R. Daly, A. T. Radosevich, *Angew. Chem. Int. Ed.* **2019**, *58*, 6993–6998; *Angew. Chem.* **2019**, *131*, 7067–7072.
- [3] a) D. Tanaka, Y. Kadonaga, Y. Manabe, K. Fukase, S. Sasaya, H. Maruyama, S. Nishimura, M. Yanagihara, A. Konishi, M. Yasuda, *J. Am. Chem. Soc.* **2019**, *141*, 17466–17471; b) H. Zhu, E. Y. X. Chen, *Inorg. Chem.* **2007**, *46*, 1481–1487; c) A. Chardon, A. Osi, D. Mahaut, T. H. Doan, N. Tumanov, J. Wouters, L. Fusaro, B. Champagne, G. Berionni, *Angew. Chem. Int. Ed.* **2020**, *59*, 12402–12406; *Angew. Chem.* **2020**, *132*, 12502–12506.
- [4] a) L.-M. Yang, E. Ganz, Z. Chen, Z.-X. Wang, P. von Ragué Schleyer, *Angew. Chem. Int. Ed.* **2015**, *54*, 9468–9501; *Angew. Chem.* **2015**, *127*, 9602–9637; b) D. Röttger, G. Erker, *Angew. Chem. Int. Ed. Engl.* **1997**, *36*, 812–827; *Angew. Chem.* **1997**, *109*, 840–856; c) M. Menzel, D. Steiner, H.-J. Winkler, D. Schweikart, S. Mehle, S. Fau, G. Frenking, W. Massa, A. Berndt, *Angew. Chem. Int. Ed. Engl.* **1995**, *34*, 327–329; *Angew. Chem.* **1995**, *107*, 368–370.
- [5] a) C. Präsang, M. Hofmann, G. Geiseler, W. Massa, A. Berndt, *Angew. Chem. Int. Ed.* **2002**, *41*, 1526–1529; *Angew. Chem.* **2002**, *114*, 1597–1599; b) E. J. Thompson, T. W. Myers, L. A. Berben, *Angew. Chem. Int. Ed.* **2014**, *53*, 14132–14134; *Angew. Chem.* **2014**, *126*, 14356–14358; c) M. Driess, J. Aust, K. Merz, C. van Wullen, *Angew. Chem. Int. Ed.* **1999**, *38*, 3677–3680; *Angew. Chem.* **1999**, *111*, 3967–3970.
- [6] M. B. Krogh-Jespersen, J. Chandrasekhar, E. U. Wuerthwein, J. B. Collins, P. von Ragué Schleyer, *J. Am. Chem. Soc.* **1980**, *102*, 2263–2268.
- [7] a) F. Ebner, H. Wadepohl, L. Greb, *J. Am. Chem. Soc.* **2019**, *141*, 18009–18012; b) F. Ebner, L. Greb, *J. Am. Chem. Soc.* **2018**, *140*, 17409–17412.
- [8] a) A. Bauzá, A. Frontera, T. J. Mooibroek, *Nat. Commun.* **2017**, *8*, 14522; b) M. Mayer, V. van Lessen, M. Rohdenburg, G.-L. Hou, Z. Yang, R. M. Exner, E. Aprà, V. A. Azov, S. Grabowsky, S. S. Xantheas, K. R. Asmis, X.-B. Wang, C. Jenne, J. Warneke, *Proc. Natl. Acad. Sci. USA* **2019**, *116*, 8167–8172; c) J. M. Holthoff, E. Engelage, R. Weiss, S. M. Huber, *Angew. Chem. Int. Ed.* **2020**, *59*, 11150–11157; *Angew. Chem.* **2020**, *132*, 11244–11251.
- [9] F. Ebner, L. M. Sigmund, L. Greb, *Angew. Chem. Int. Ed.* **2020**, *59*, 17118–17124; *Angew. Chem.* **2020**, *132*, 17266–17272.
- [10] L. M. Sigmund, L. Greb, *Chem. Sci.* **2020**, *11*, 9611–9616.
- [11] a) L. Greb, F. Ebner, Y. Ginzburg, L. M. Sigmund, *Eur. J. Inorg. Chem.* **2020**, 3030–3047; b) E. R. M. Habraken, A. R. Jupp, M. B. Brands, M. Nieger, A. W. Ehlers, J. C. Slootweg, *Eur. J. Inorg. Chem.* **2019**, 2436–2442; c) U. Gellrich, M. Hasenbeck, *Chem. Eur. J.* **2021**, <https://doi.org/10.1002/chem.202004563>.
- [12] L. Yang, D. R. Powell, R. P. Houser, *Dalton Trans.* **2007**, 955–964.
- [13] a) S. Grimme, J. G. Brandenburg, C. Bannwarth, A. Hansen, *J. Chem. Phys.* **2015**, *143*, 054107; b) Y. Zhao, D. G. Truhlar, *J. Phys. Chem. A* **2005**, *109*, 5656–5667; c) F. Weigend, R. Ahlrichs, *Phys. Chem. Chem. Phys.* **2005**, *7*, 3297–3305; d) S. Grimme, S. Ehrlich, L. Goerigk, *J. Comput. Chem.* **2011**, *32*, 1456–1465; e) A. D. Becke, E. R. Johnson, *J. Chem. Phys.* **2005**, *123*, 024101; f) A. Klamt, G. Schuurmann, *J. Chem. Soc. Perkin Trans. 2* **1993**, 799–805; g) C. C. Pye, T. Ziegler, *Theor. Chem. Acc.* **1999**, *101*, 396–408.
- [14] a) M. von Hopffgarten, G. Frenking, *Wiley Interdiscip. Rev.: Comput. Mol. Sci.* **2012**, *2*, 43–62; b) L. Zhao, M. von Hopffgarten, D. M. Andrada, G. Frenking, *Wiley Interdiscip. Rev. Comput. Mol. Sci.* **2018**, *8*, e1345.
- [15] R. W. Hoffmann, *Chem. Rev.* **1989**, *89*, 1841–1860.

Manuscript received: December 28, 2020

Accepted manuscript online: January 22, 2021

Version of record online: February 24, 2021